Electrochimica Acta 435 (2022) 141428

Contents lists available at ScienceDirect

Electrochimica Acta

journal homepage: www.journals.elsevier.com/electrochimica-acta

Electrodeposition of CoNi alloys in a biocompatible DES and its suitability for activating the formation of sulfate radicals

Elvira Gómez [a,b,*], Arnau Fons [a], Roberto Cestaro [c], Albert Serrà [a,b,*]

[a] Grup d'Electrodeposició de Capes Primes i Nanoestructures (GE-CPN), Departament de Ciència de Materials i Química Física, Universitat de Barcelona, Martí i Franquès, 1, Barcelona, Catalonia E-08028, Spain
[b] Institute of Nanoscience and Nanotechnology (IN2UB), Universitat de Barcelona, Barcelona, Catalonia, Spain
[c] Laboratory for Joining Technologies and Corrosion, Empa Swiss Federal Laboratories for Materials Science and Technology, Dübendorf CH-8600, Switzerland

ARTICLE INFO

Keywords:
CoNi electrodeposition
DES solvent
Characterization
Sulphate radical

ABSTRACT

Building a sustainable future requires new, accessible, economic, and ecological methods of preparing nanostructured materials used in biomedical and environmental applications. In this work, a detailed study on the electrodeposition process of CoNi in a biocompatible deep eutectic solvent (DES) is presented. Alloy plating performed in choline chloride within a urea-based DES allowed us to tailor elemental compositions, morphologies, and size of the deposits based on the plating conditions. Homogeneous, continuous, and needle-shaped deposits were characterized using electrochemical methods and *ex-situ* characterization techniques. Although the process's electrochemical behavior corresponded to that of normal deposition, applying the most negative potentials produced a co-reduction of the solvent, which favored the incorporation of oxygen species into the deposit. Given the materials' nature, morphology, and composition tailored to the high active surface, the materials were tested as platforms to activate the formation of sulfate radicals from the peroxomonosulfate salt. Results related to the proposed material and preparation method were promising, as, confirmed by the high effectiveness in degrading the antibiotic tetracycline. Altogether, the work showcases a versatile, environmentally friendly route for electrodepositing CoNi in DESs to yield a proactive tool for developing of platforms with catalytic potential.

1. Introduction

Ferromagnetic materials have always had wide-ranging applications given their properties that make them multifunctional. Whereas older applications were largely decorative, or protective due to the materials' high resistance to corrosion, they have more recently been incorporated into microelectromechanical systems, in which their inherent soft-magnetic character provides a rapid response to magnetic fields and their durability gives devices long lifetimes of use [1–4].

In past years, the intense rise of developments involving heterogeneous catalytic processes has galvanized the search for new materials that behave similarly to traditional catalysts. However, considering the conventional incorporation of high-cost precious or rare metals in traditional catalysts, the objective has been to identify more abundant materials that can achieve similar efficiency but in a more economical way [5–7]. To that end, ferromagnetic-based materials have proven to be good candidates as non-precious catalysts whose versatility allows to promote favorable conditions in different types of processes [5,6,8].

Although applications of ferromagnetic-based materials, especially nickel-based ones, have been consolidated in the production and accumulation of energy, as well as extended to electrochromism due to their capacity for optical modulation, they continue to regularly expand [9, 10]. Among the ferromagnetic materials, cobalt–nickel (CoNi) alloys are versatile alloys widely used in energetic materials, magnetic materials, catalytic materials, and decorative coatings given their outstanding performance in light absorption, magnetism, catalysis and high resistance to corrosion [11–15]. Among the procedures for preparing CoNi alloys, electrodeposition provides a strong, powerful method to synthesize defined alloys using simple and inexpensive equipment to modulate the composition by tailoring the electrodeposition conditions [3,11,16–18].

To date, the electrodeposition of CoNi has been developed in

* Corresponding authors at: Grup d'Electrodeposició de Capes Primes i Nanoestructures (GE-CPN), Departament de Ciència de Materials i Química Física, Universitat de Barcelona, Martí i Franquès, 1, Barcelona, Catalonia E-08028, Spain.
E-mail addresses: e.gomez@ub.edu (E. Gómez), a.serra@ub.edu (A. Serrà).

https://doi.org/10.1016/j.electacta.2022.141428
Received 1 August 2022; Received in revised form 21 October 2022; Accepted 21 October 2022
Available online 23 October 2022

aqueous baths using electroactive salts based on chloride, acetate, or sulfate compounds. Although aqueous media provide a sufficient electrochemical window, activity towards the hydrogen evolution reaction (HER) of both metals, and consequently their alloys compromises the quality of the obtained deposits due to the simultaneous hydrogen's codeposition [11,18–20]. To minimize this side-effect, essential additives are usually necessary to modify the electrodeposition process and achieve the desired coating quality. Some such additives are organic species that require severe concentration control to ensure the bath's stability and may be dangerous for the environment [14,21]. Moreover, anomalous CoNi codeposition in aqueous media involves preferentially depositing the less noble metal (i.e., cobalt), thereby forcing the use of high Ni(II):Co(II) concentration ratios in order to prepare deposits with high nickel content. Beyond that, using aqueous media generates large amounts of polluting wastewater that subsequently has to be recycled [3,14,15,17–19].

In response to the inherent drawbacks of CoNi alloy deposition in aqueous media, efforts to replace the method remain ongoing, especially with sustainable and economical media able to overcome hydrogen formation and losses of efficiency and circumvent the use of toxic chemicals. After several attempts using expensive, unwieldy room temperature ionic liquids (RTIL) in the last decade, a proposal was made to use deep eutectic solvents (DES), solvent–electrolyte media consisting of quaternary ammonium salts mixed with a hydrogen bond donor [22–25]. DESs are insensitive to moisture or air, exhibit good conductivity, chemical and thermal stability, and an electrochemical window larger than water's [26]. Moreover, DESs are easy to prepare, environmental friendly, biodegradable, and affordable, all of which make them suitable for research involving electrodeposition [6,8,27–29]. However, since 2012, few attempts have been made to evaluate CoNi electrodeposition using either RTIL-choline chloride mixtures or a true DES, and all deposition processes were studied under restricted conditions that did not afford an overall picture of the process [16,21,24,30–33].

This work is devoted to gain knowledge of CoNi deposition in DESs and to identify the influence of different electrodeposition parameters in the overall concentration range. First, in order to deepen the understanding on the electrochemical behavior, glassy carbon was selected as electrode to allow a straightforward investigation of the electrodeposition processes and to transfer the results to more complex substrates. Considering that our final application purpose is the use of the CoNi alloy in different heterogeneous catalytic processes, the process was characterized on Si/Ti/Au substrates. The objective is to evaluate the possible contribution of the electrodeposition conditions to the enhancing of the effective surface, a factor that, after its catalytic power, must be taken into account for a catalyst.

The selected DES was the one formed by the mixture choline chloride and urea (CU) in a 1:2 molar ratio (previously used for the electrodeposition of single ferromagnetic metals) [25,29,34]. Due to the nature of its constituents, it is relatively easy to maintain the system in anhydrous conditions. Minimizing the incorporation of water is important because its presence can be detrimental for the final quality of the deposit. CU is a relatively common high viscosity DES, which can slow down transport processes, thus favoring an increase of the roughness of the prepared deposit in certain conditions [2,35,36].

CoNi deposition was analyzed under different conditions of electrodeposition. Four concentration ratios [Co(II)]/[(Ni(II)] were analyzed with cyclic voltammetry, voltammetric-potential hold, and potentiostatic techniques in a wide range of applied potential. The samples were characterized in order to gain the information needed to establish the behavior of the electrodeposition process and evaluate the characteristics of the deposits as a function of the process's conditions. The morphology of the deposits was characterized by field emission scanning electron microscopy (FE-SEM). The compositional analysis was examined by electron dispersive microscopy (EDS), X-ray photoelectron spectroscopy (XPS) and induced coupled plasma (ICP) – mass spectroscopy (MS). Some of the deposits prepared were also structurally characterized by X-ray diffraction (XRD). The work also investigates the possible effect of solvent's co-reduction on the characteristics of prepared deposits.

As a concept probe, the prepared substrates were tested as tools for activating a reagent capable of generating effective oxidative radicals—in this case, peroxomonosulfate (PMS) —that can participate in oxidizing complex organic molecules [37–40]. These results have the potential to open a new field of application for CoNi materials in processes for degrading recalcitrant organic pollutants.

Table 1
Composition of baths analyzed.

Plating bath	Identification	$CoCl_2$ /M	$NiCl_2$ /M
1	**7Co10Ni**	0.07	0.1
2	**10Co7Ni**	0.1	0.07
3	**14Co3Ni**	0.14	0.03
4	**3Co14Ni**	0.03	0.14

2. Experimental

Electrochemical experiments were performed in a thermostatized three-electrode system. The reference electrode was Ag|AgCl|Cl mounted in a Luggin capillary containing the DES, while the counter electrode was a platinum spiral. The counter platinum spiral was immersed in a concentrated nitric acid solution, cleaned by flame annealing, and, once cooled, immersed in the solution. Two working electrodes were used: a glassy carbon (GC) rod (0.0314 cm^2), and flat silicon pieces with a seed layer containing Ti (15 nm) and Au (100 nm), hereinafter called "Si/Ti/Au" (0.30 cm^2). The Au layer acts as a seed layer to improve conductivity and facilitate the nucleation of co-deposits. The glassy carbon electrode was polished to a mirror finish with alumina of different grades (3.75 and 1.87 μm; VWR Prolabo), cleaned ultrasonically for 2 min in water treated with the Milli Q system, and dried with nitrogen prior to immersion in the solution. The Si/Ti/Au pieces were cleaned exhaustively with ethanol and acetone, and electrochemical measurements were performed using an Autolab with PGSTAT30 equipment and GPES software.

The DES was prepared using choline chloride (ChCl, Across Organics) and urea (Merck) both reagents of analytical-grade. ChCl was dried in an oven at 70 °C for 48 h and placed in a desiccator, after which the DES was prepared by mixing amounts of ChCl and urea in a 1:2 ChCl: urea molar proportion, warmed at approximately 50 °C, and stirred continuously until becoming a colorless liquid typical of DES [41,42]. The liquid was maintained overnight under vacuum, stirring, and heating conditions ($T < 50$ °C) to reduce the water content until the optimal potential window was achieved. Prior to preparing the electroactive solutions, $CoCl_2$ hexahydrate from Alfa Aesar and $NiCl_2$ hexahydrate from Merck, both of analytical grade, were dried at 105 °C for 24 h until dehydration. To dissolve the Co(ll) and Ni(ll) salts in the DES, the mixture was stirred and heated at approximately 50 °C overnight and subsequently kept in an argon atmosphere. Four solutions with different [Co(II)]/[Ni(II)] ratios were prepared in which the total concentration of the electroactive species was arbitrarily fixed at 0.17 M. The relative molar concentrations are shown in Table 1. The solutions were deoxygenated with argon before experiments and subsequently maintained in an argon atmosphere throughout the experiments. Unless stated otherwise, all experiments were performed on freshly prepared surfaces, and the solution's working temperature was kept at 70 °C.

The deposits were potentiostatically prepared using Autolab with PGSTAT30 equipment and GPES software, with a total circulated charge of 15 mC and 150 mC for the glassy carbon and Si/Ti/Au substrates, respectively. The morphology of the samples was analyzed using FE-SEM (JSM-7100F Analytical Microscope), which incorporates an X-ray analyzer that allows the compositional characterization of the samples prepared using the EDS technique operating at 20 kV. The EDS system

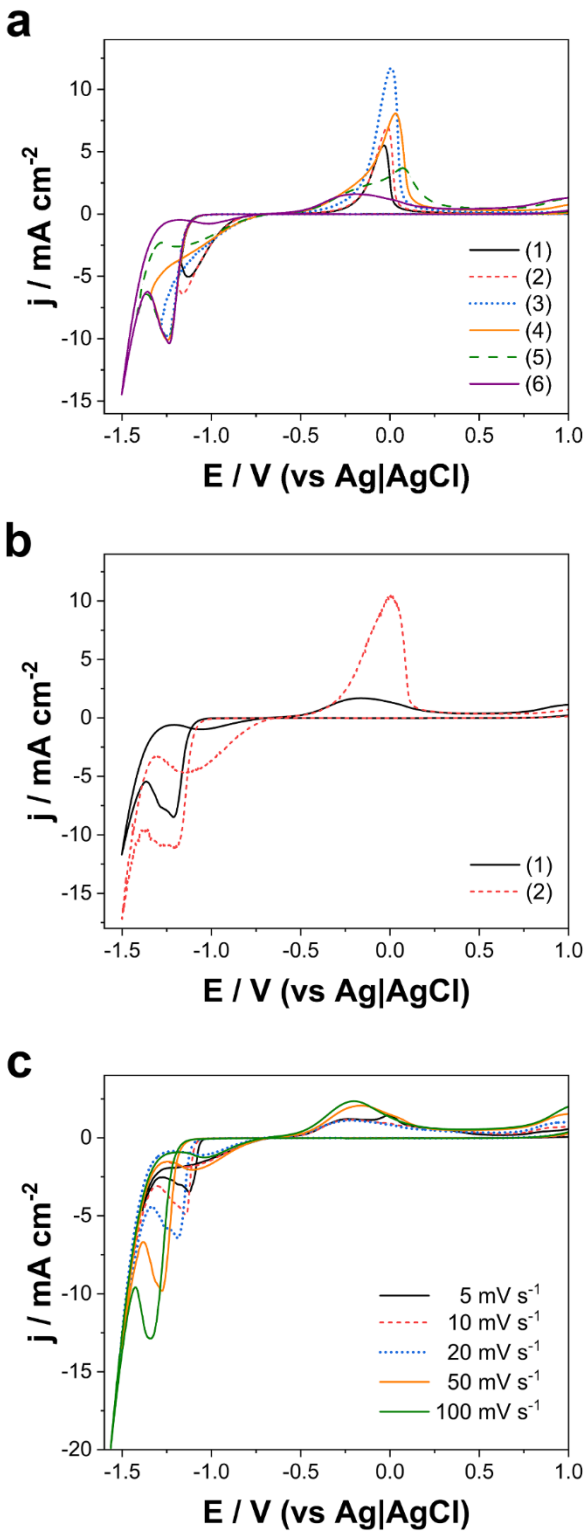

Fig. 1. Cyclic voltammetries recorded at 50 mV s^{-1} for the plating bath 1 on glassy carbon (a) at different cathodic potential limits: −1.17 V (curve 1); −1.19 V (curve 2); −1.28 V (curve 3); −1.34 V (curve 4); −1.42 V (curve 5); and −1.50 V (curve 6); (b) at a cathodic potential limit of −1.50 V under stationary (curve 1) and nonstationary – magnetic stirring (curves 2) conditions. (c) Cyclic voltammetries for the plating bath 1 on glassy carbon at different scan rate.

was previously calibrated using a pure cobalt standard. EDS compositional analysis was performed at a minimum of five points of the sample considering the center and the corners of the deposit, and the deposit's composition was confirmed using chemical analysis. Films were dissolved in 1% nitric acid, and the resulting solutions were analyzed by inductively coupled plasma mass spectrometry (ICP-MS; Perkin-Elmer spectrometer Elan 6000). The thickness of films was determined using a 3D optical surface metrology system (Leica DCM 3D). XPS measurements were taken with an XPS system (PHI 5600 Multitechnique, Physical Electronics) using a monochromatic X-ray source (Al K αline = 1486.6 eV, 350 W). The area analyzed was a circle 0.8 mm in diameter, and all measurements were made in an ultra-high vacuum chamber. The compositional profile of the CoNi deposits was obtained by etching by means of argon ion sputtering up to a few nanometers prior to acquiring angle-resolved XPS images. MultiPak 8.2 was used to acquire digital images and to perform peak deconvolution. XRD patterns were recorded using a X-ray diffraction (XRD, Bruker D8 Discovery diffractometer) in the Bragg–Brentano configuration, Cu K_α radiation (λ=0.1542 nm). A 2θ scan, between 20 and 100°, was used, with a step size of 0.05 and a measuring time of 15 s per step. All spectra were collected using Al K_α radiation (1486.6 eV).

Before characterization, all samples were cleaned thoroughly with warm water for the time needed to entirely remove the remained DES residues on the samples.

Tests to assess the suitability of some obtained CoNi deposits for activating PMS, "Oxone", which contains ($KHSO_5 \cdot 0.5KHSO_4 \cdot 0.5K_2SO_4$; Merck) as generating oxidative radical species able to degrade and mineralize tetracycline (TC, Alfa Aesar), were performed at room temperature, using 3 mL of TC solutions of 20 ppm and PMS concentrations of 0.3 mM. TC absorbance was recorded using a UV-1800 Shimadzu spectrophotometer, and the associated mineralization was evaluated by determining the total organic content (TOC) in the solution (TOC-V_{CSH} Shimadzu equipment). To gauge the reusability of the most efficient substrate, the catalysts were reused in 10 consecutive experiments.

3. Results

3.1. Electrochemical analysis using vitreous carbon substrate

First, for all solutions, voltammetric experiments were performed on vitreous carbon at different potential limits in order to establish the general trends of the deposition process. Fig. 1a shows the recorded cyclic voltammograms from the 7Co10Ni plating bath conducted at different negative potential limits. The electrochemical window of the glassy carbon and DES blank solution (i.e., without the metallic precursor) is shown in Fig. S1a. When the cathodic potential limit is -1.17 V, the recorded current loop in the positive branch (Fig. 1a, curve 1) confirms that the bulk deposition of CoNi in DES requires a significant overpotential to initiate the process, which corresponds to the nucleation and growth process [30,32,43]. The appearance of the oxidation peak is associated with the oxidation of the deposited product; no other remarkable oxidation current was observed. Increasing the negative potential limit, the recorded current develops a clear reduction peak, which counters the broader and more intense oxidation peak in the positive scan, involving a larger deposition charge, as expected (Fig. 1a, curve 2). However, by enlarging the scan to a more negative potential value, at which more evident peak feature is observed (Fig. 1a, curve 3), an unexpected and not previously reported result for CoNi deposition in DES is observed. The recorded oxidation current profile was broader nonsymmetrical and the involved Q_{ox}/Q_{red} ratio diminished considerably by scanning toward a more positive potential incipient oxidation band, which appeared before the massive oxidation current. Following the scan further to a more negative potential, a massive reduction current appeared, predictably related to the solvent reduction; in addition, an even more negative cathodic limit lead to a more pronounced

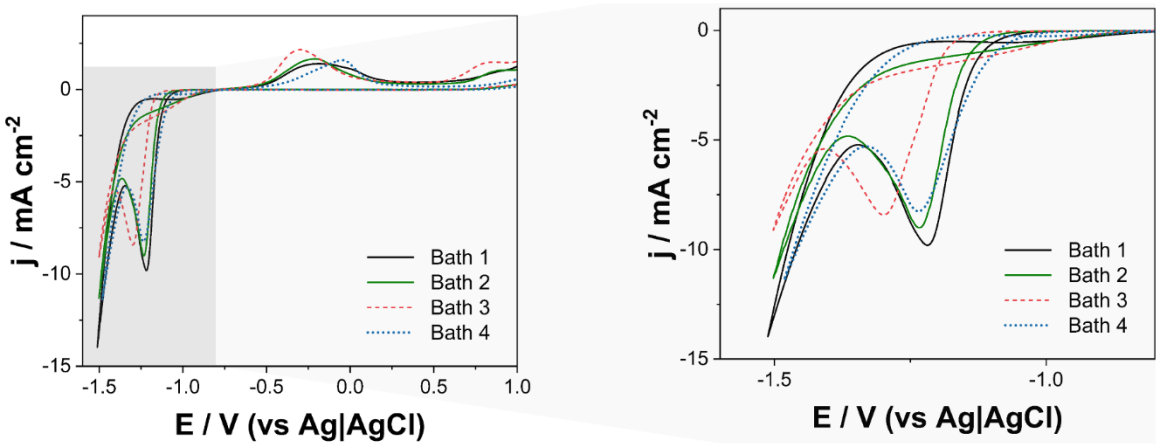

Fig. 2. Cyclic voltammetries recorded at 50 mV s^{-1} on glassy carbon for the four plating baths described in Table 1.

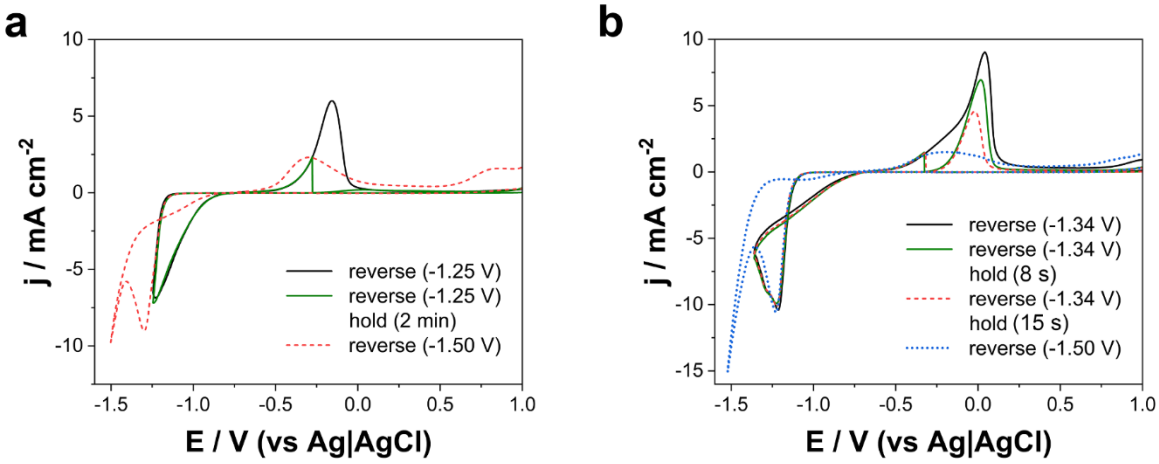

Fig. 3. Cyclic voltammetries recorded at 50 mV s^{-1} on glassy carbon, with and without voltammetric holds, in the positive scan for (a) plating bath 3 and (b) plating bath 4.

broadening of the oxidation current and loosening of the Q_{ox}/Q_{red} ratio (Fig. 1a, curves 5 and 6).

To extract complementary information on the deposition process, the influence of solution stirring was investigated. Fig. 1b shows the comparison between the voltammograms recorded under stationary conditions (Fig. 1b, curve 1) and agitated conditions (Fig. 1b, curve 2). The reduction branch shows that, under agitation, the current involved is greater, corresponding to a mass-influenced process. The most relevant information, however, resides in the different behavior in the Q_{ox}/Q_{red} current ratio recorded under agitation conditions, for which the clear decrease in oxidation current is not observed. In addition, experiments at different scan rates (Fig. 1c) evidence that, as the scan rates decrease, the current appearance revealed at more positive potentials for being a lower current peak. Another feature that can be seen from the recorded curves is that, as the scanning rate decreases, an incipient splitting of the reduction peak seems to be detected.

Fig. 2 shows the voltammograms recorded at 50 mV s^{-1} from each one of the baths studied. For the four solutions analyzed a similar voltammetric behavior was observed, specifically: (i) typical nucleation loop, (ii) favorable influence of solution agitation and (iii) pernicious effect on the oxidation peak current using scanning limits that promote the reduction of the medium. Similar voltammetric behavior was previously reported in the same DES for cobalt- and nickel-free baths but using a lower cobalt or nickel salt concentration, respectively [29,44]. For each solution, the appearance of the voltammetric current was a function of the composition, as the content of Co(II) in the solution increases the onset of the reduction current was delayed to more negative potentials.

To electrochemically characterize the deposit formed during the voltammetric scan, experiments involving voltammetric holds in the positive scan were performed. The chosen experiment consists in stopping the scan for a controlled time at a potential value in the range of the oxidation peak, after which the scan is continued. The comparison between the voltammetric response involving a potential hold with respect to a normal potential scan provides information about the type of deposit formed (Fig. 3). At first, holding potential experiments were performed in which the potential was reversed in short limits after the nucleation, from which the deposit mainly was formed during the loop. The results show that by stopping the scan, even in the rising part of the oxidation peak, the recorded current profile shows inappreciable values, indicating that complete oxidation has occurred (Fig. 3a).

For voltammetric experiments in which the scan was reversed after the peak, but prior the main reduction of the solvent, holding the potential at the beginning of the oxidation peak for a relatively short time, 8 and 15 s (Fig. 3b), resulted in a progressive decrease of the oxidation peak intensity (peak potential moves slightly and the width of the peak is reduced). As a consequence, the current becomes almost zero at less positive potentials. Prolonging the oxidation time to 2 min, it is observed that only residual current is recorded in the potential range of the oxidation peak, and no new features appeared at more positive potentials. These results seem to indicate that a single homogeneous system as a solid solution, is formed, although this must be confirmed by the

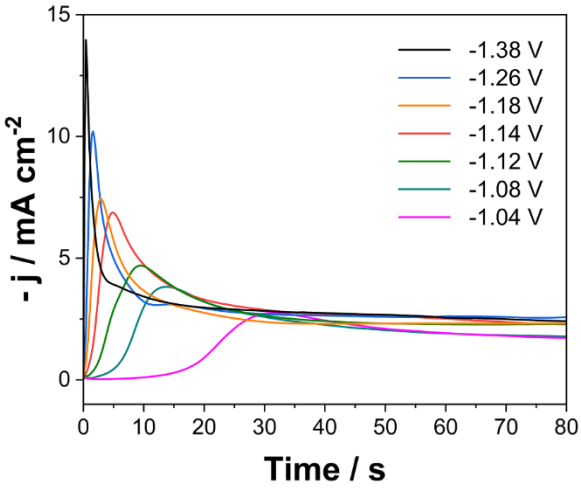

Fig. 4. Chronoamperometric transients of the CoNi deposition on glassy carbon from plating bath 3 at different applied potentials.

posterior structural characterization. The same behavior was observed in all four plating baths.

Potentiostatic experiments were performed, increasing the potential from a value at which no-process is done to different potentials at which codeposition takes place. For all the baths, the applied potential values were selected from the previous voltammetric results. The recorded current confirms the nucleation and 3D growth process, as a current peak emerges in the profile whose maximum appears earlier and reveals the more negative potential (Fig. 4). However, to overcome the maximum, in the curved recorded from the most negative potentials, it is observed that some other factor, other than mass transport, also contributes to the current decrease. The drop-in current is abrupt; further, at longer deposition times the current value is greater than that corresponding to the monotonical diminution observed at the less negative potentials. This behavior matches well with the progressive diminution in the recorded oxidation current observed in voltammetric experiments in which, at sufficient negative potential range, some new reduction processes lead to hindering the deposit's growth and oxidation ability. No other interpretation could be advanced due to the deposition process involving cobalt and nickel, which exhibit dissimilar electrochemical behavior.

3.2. Electrochemical study using Si/Ti/Au substrate

To analyze the possible influence of the substrate's nature on the deposition process, voltammetric curves on Si/Ti/Au pieces were recorded extending the scan even to potentials corresponding to the massive DES reduction, for comparison with that obtained from the vitreous carbon substrate. As shown in Fig. S1b, the electrochemical window of Si/Ti/Au in DES was considerably shorter than that on glassy carbon. On the Si/Ti/Au substrate, the appearance of the reduction current is slightly advanced; further, the semiconductor character of the main layer is compensated by the seed gold layer's presence. A voltammetric behavior similar to that recorded on vitreous carbon was observed, noting a specific potential range from which pernicious secondary reactions take place, an effect minimized under stirring conditions (Fig. S2).

For all four baths, the different current-time (j-t) transients recorded on Si/Ti/Au substrate, show at stationary conditions a similar behavior to that observed on vitreous carbon, in which the slope of the j-t transient increases and peak maximum appears at short times when the applied potential was made more negative. In order to check the influence of mass transfer, experiments were performed in which the solution was stirred by moderately flowing argon gas after a deposition period (Fig. 5). In these conditions, the sudden current increase was recorded, i.e., a current that maintained in quasi-constant value, corresponding to a process in which the contribution of electroactive species is relevant.

3.3. Electrodeposition of CoNi nanostructured films

For each of the four baths studied, electrodeposited films were prepared on both vitreous carbon and Si/Ti/Au substrates in a specific range of potentials depending on the bath. Continuous agitation of the electrolyte allowed avoiding possible compositional gradients throughout the deposit's thickness.

Compositional analysis carried out using the EDS technique on the films obtained from the same solution (Table 2) shows that the atomic cobalt content is highly dependent on the electrolyte nature. ICP-MS analysis confirmed the compositional results, which were slightly higher than the ones obtained by EDS analysis but nevertheless revealed a similar tendency. Indeed, the CoNi electrodeposition process corresponds to a normal electrodeposition process in DES, while the less noble metal is preferentially deposited in an aqueous medium.

The current efficiency (CE) depends as much on the relative ratio of cobalt and nickel as on the applied potential. In our study, the baths with a higher concentration of cobalt had slightly lower efficiencies than the nickel baths. At the same time, as expected, because the deposition

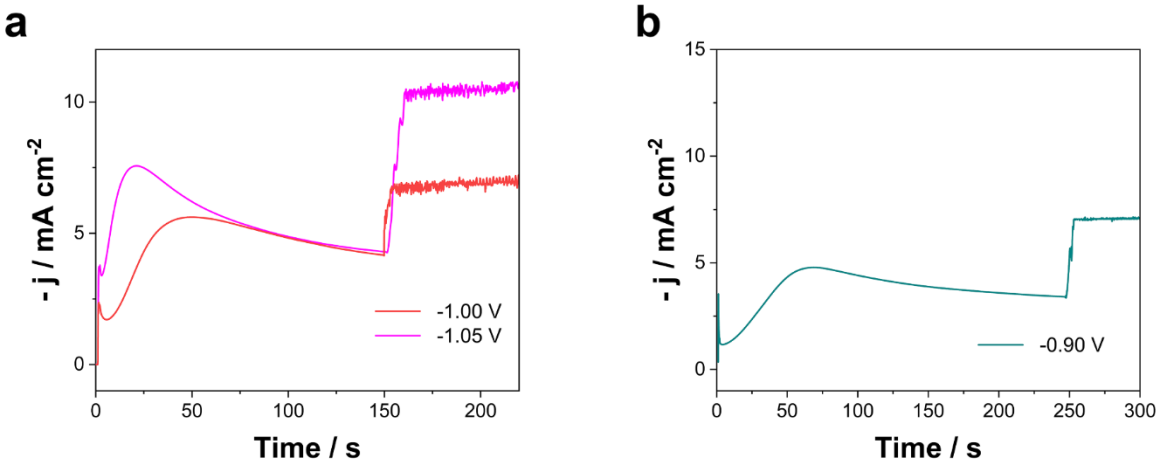

Fig. 5. Chronoamperometric transients of the CoNi deposition on Si/Ti/Au at different applied potentials from (a) plating bath 3 (magnetic stirring started at 150 s) 150 s, and (b) plating bath 4 (magnetic stirring started at 250 s).

Table 2
Atomic cobalt content and current efficiency of electrodeposited films prepared at different potentials using the four plating baths on vitreous glassy carbon and Si/Ti/Au electrodes.

	Plating bath 1 7Co10Ni			Plating bath 2 10Co7Ni			Plating bath 3 14Co3Ni			Plating bath 4 3Co14Ni		
Vitreous carbon	-1.03 V			-0.98 V			-1.10 V			-1.03 V		
	EDS (at. Co %)	ICP (at. Co %)	CE / %	EDS (at. Co %)	ICP (at. Co %)	CE / %	EDS (at. Co %)	ICP (at. Co %)	CE / %	EDS (at. Co %)	ICP (at. Co %)	CE / %
	49	50.2	85	56	56.8	90	86	85.8	85	18	18.2	80
	-1.04 V			-1.01 V			-1.18 V			-1.06 V		
	EDS (at. Co %)	ICP (at. Co %)	CE / %	EDS (at. Co %)	ICP (at. Co %)	CE / %	EDS (at. Co %)	ICP (at. Co %)	CE / %	EDS (at. Co %)	ICP (at. Co %)	CE / %
	47	48.1	82	62	60.8	86	86	86.1	78	20	19.5	76
	-1.05 V			-1.04 V			-1.30 V			-1.09 V		
	EDS (at. Co %)	ICP (at. Co %)	CE / %	EDS (at. Co %)	ICP (at. Co %)	CE / %	EDS (at. Co %)	ICP (at. Co %)	CE / %	EDS (at. Co %)	ICP (at. Co %)	CE / %
	45	47.1	80	55	56.7	80	86	86.7	60	20	20.8	70
	-1.07 V			-1.07 V						-1.18 V		
	EDS (at. Co %)	ICP (at. Co %)	CE / %	EDS (at. Co %)	ICP (at. Co %)	CE / %				EDS (at. Co %)	ICP (at. Co %)	CE / %
	44	45.6	75	61	62.1	77				21	22.1	58
				-1.10 V								
				EDS (at. Co %)	ICP (at. Co %)	CE / %						
				61	62.1	73						
Si/Ti/Au				-1.02 V			-1.02 V			-0.90 V		
				EDS (at. Co %)	ICP (at. Co %)	CE / %	EDS (at. Co %)	ICP (at. Co %)	CE / %	EDS (at. Co %)	ICP (at. Co %)	CE / %
				56	56.4	85	86	83.8	85	8	8.6	84
				-1.04 V			-1.03 V			-0.93 V		
				EDS (at. Co %)	ICP (at. Co %)	CE / %	EDS (at. Co %)	ICP (at. Co %)	CE / %	EDS (at. Co %)	ICP (at. Co %)	CE / %
				66	66.6	78	86	83.8	80	11	11.8	80
				-1.06 V			-1.05 V			-0.95 V		
				EDS (at. Co %)	ICP (at. Co %)	CE / %	EDS (at. Co %)	ICP (at. Co %)	CE / %	EDS (at. Co %)	ICP (at. Co %)	CE / %
				65	64.7	77	85	84.2	73	13	14.2	80
										-1.08 V		
										EDS (at. Co %)	ICP (at. Co %)	CE / %
										29	26.2	70
										-1.15 V		
										EDS (at. Co %)	ICP (at. Co %)	CE / %
										23	23.7	63
										-1.25 V		
										EDS (at. Co %)	ICP (at. Co %)	CE / %
										23	23.8	55

potential was more negative, the efficiency was lower. Those two trends were applicable to both types of substrates. Despite the higher conductivity of the Si/Ti/Au substrate, there was no quantifiable improvement in the efficiency of the electrodeposition process. In all cases, deposits with thicknesses between approximately 150 and 240 μm, depending on the current efficiency, were obtained.

The Co-rich solution (bath 3 – 3Ni14Co) leads to deposits in which the nickel percentage varies hardly with the applied potential. On the other hand, more sensitive compositional changes occur by varying the applied potential in the Ni-rich solution (bath 4 – 14Ni3Co): the cobalt percentage in the deposit increases progressively as applied potential is more negative. From the intermediate solutions the effect of the diminution of the applied potential (more negative values) follows, as expected.

FE-SEM images of the deposits prepared on vitreous carbon (Fig. 6) show that a similar surface morphology was obtained independently on the selected potential range and electrolyte. Deposits are compact and homogeneous, having thin platelets with a randomly distributed sharper edges, oriented vertically to the surface, thereby appearing to be interwoven. The grains form a network structure with a needle morphology, which appears to slightly reduce their size as the nickel content in the deposit increases, i.e., a fact that is evident comparing Ni-rich and Co-rich deposits obtained at moderate potentials. It is confirmed that in the DES medium the needle morphology is attained even in deposits with nonrelevant cobalt percentages, i.e., a fact that it is not attained in an aqueous medium, in which the characteristic desert rose morphology of the cobalt does not maintain at conditions *via* the majority nickel content [19]. This characteristic morphology could be favored by the slow-down growth rate favored by the higher viscosity of the medium.

The morphology observed for the deposits obtained on Si/Ti/Au (Fig. 7a and b) follows similar characteristics of those of the previous images of vitreous carbon; the morphology reveals the presence of clear needles that confers a fluffy aspect, which is maintained even in the deposits with low cobalt content. By contrast, deposits prepared with baths with higher content of Co and Ni electroactive species presented a similar architecture but with larger features and edges that approach to a granular morphology (Fig. 7c and d). Importantly, in both vitreous carbon (Fig. S3a) and Si/Ti/Au (Fig. S3b), applying more negative potentials leads to deposits in which the images show morphologies whose characteristics approximate more granular individual forms, i.e., morphologies that support a needle growth but to a lesser extent, especially in the Ni-rich baths.

Performance of the deposition process was also evaluated, analyzing by XPS the composition of the prepared deposits throughout the deposit profile. The expected components, cobalt and nickel, were verified along with oxygen; gold was also used to verify the possible arrival in the seed

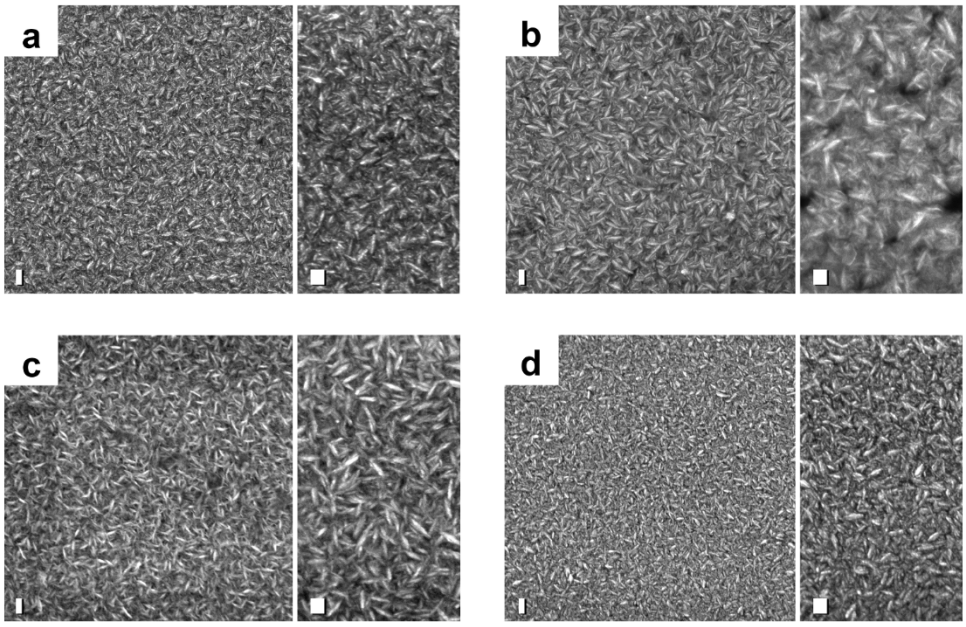

Fig. 6. FE-SEM micrographs of electrodeposits prepared on glassy carbon using (a) plating bath 1 at –1.03 V, (b) plating bath 2 at –0.98 V, (c) plating bath 3 at –1.02 V, and (d) plating bath 4 at –1.06 V. Scale bar: 100 nm.

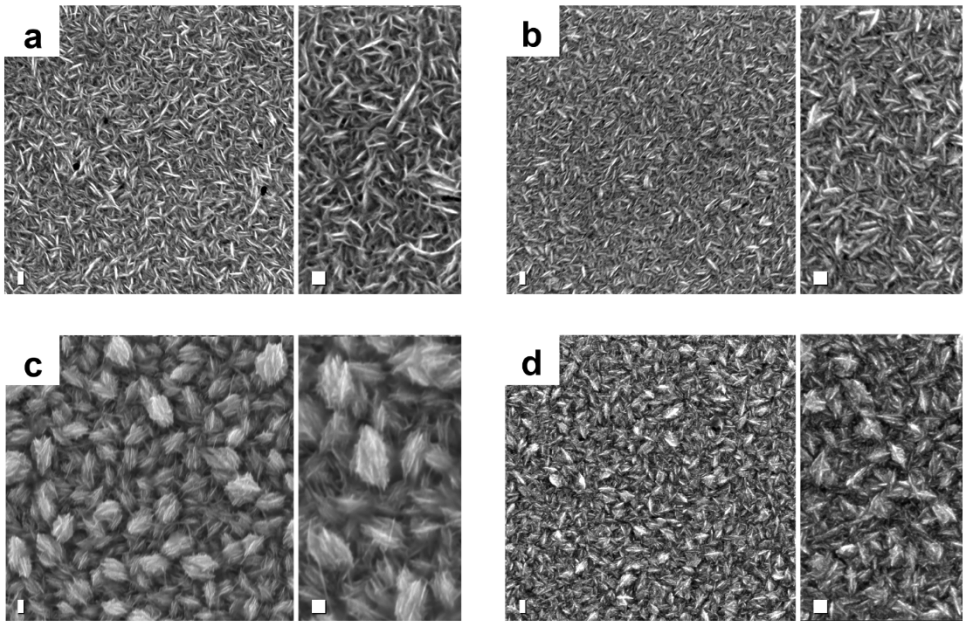

Fig. 7. FE-SEM micrographs of electrodeposits prepared on Si/Ti/Au using (a) plating bath 3 at –1.02 V, (b) plating bath 2 at –1.03 V, (c) plating bath 3 at –1.30 V, and (d) plating bath 4 at –1.06 V. Scale bar: 100 nm.

layer. However, no gold was detected in any sample, which shows that the charge involved was sufficient to achieve a sufficient number of analyses without reaching the substrate.

XPS confirms that the sample prepared at the less negative potential (Fig. 8a and c) is compositionally more homogeneous without significant oxygen content inside the deposit; when prepared at a more negative potential (Fig. 8b and d) the presence of oxygen was detected, revealing that some oxide/hydroxide content is present in the sample [45]. The last result appears to be in agreement with the voltammetric results previously obtained, in which an unexpected behavior, i.e., the diminution of the voltammetric oxidation current, was observed, thus extending the scan to potential limits overcoming the negative voltammetric peak, i.e., a behavior that could be related to secondary reaction (see Fig. 1a). Codeposition of the solvent on the CoNi freshly deposited could promote the formation of oxygen species due to the electrocatalytic character of the alloy, a reaction leading to oxides/hydroxylate species that could be responsible when they are abundant in features observed in the voltammetric curves and of the sudden current fall in the j-t transients at the more negative applied potentials [34,35]. Similar behavior was previously observed for the preparation of the nickel and cobalt deposits [29,34,35] .

Related to the preparation, from the XPS analysis, it seems that the selected procedure results are adequate to prepare homogeneous compositionally deposits using moderate potentials, which provide constancy in the composition of the metallic components. The deposit prepared at the less negative potential shows a lower oxygen content

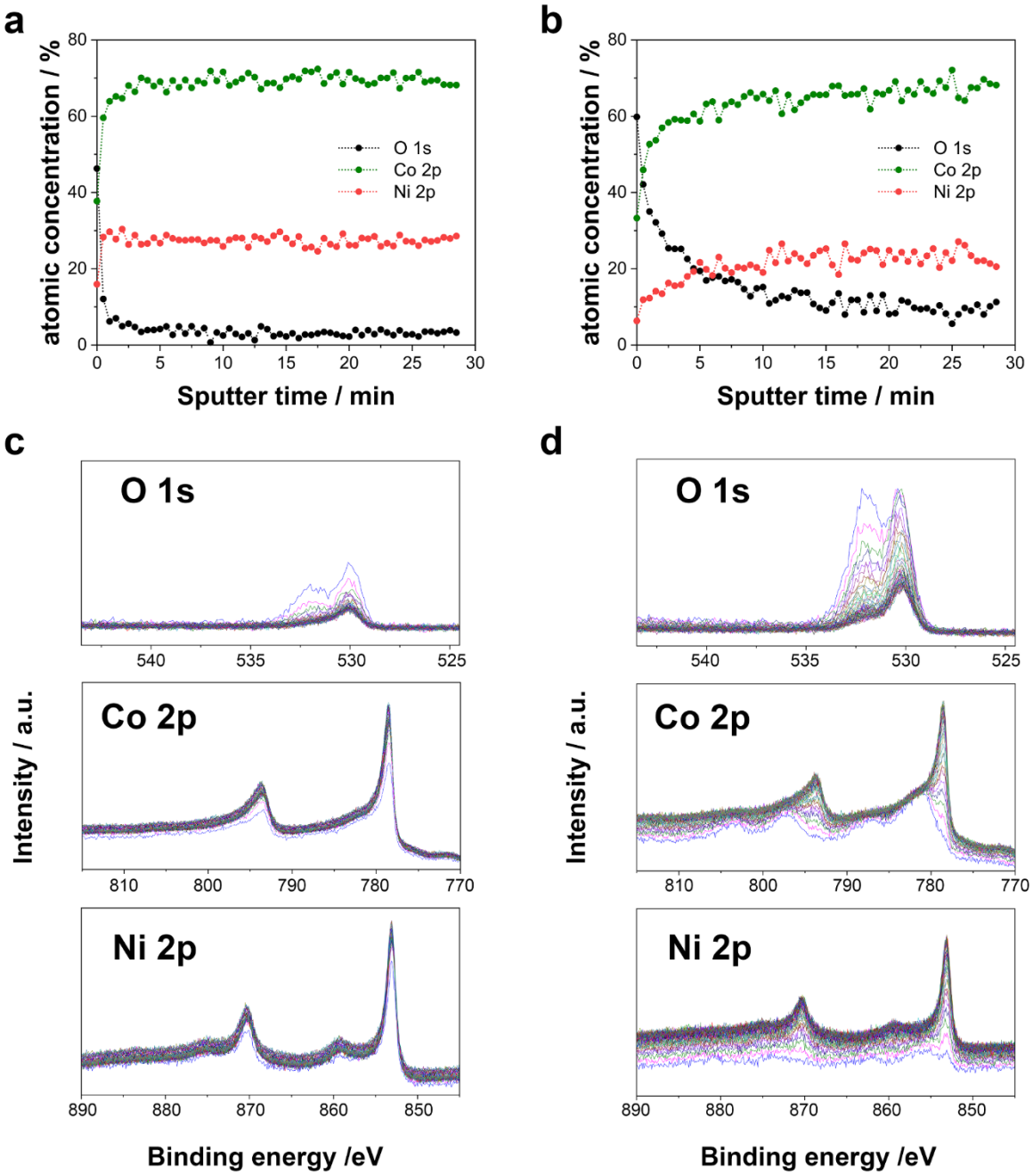

Fig. 8. Atomic elemental concentration depth profile of electrodeposited CoNi films from plating bath 2 on Si/Ti/Au electrodes at (a) –1.01 V and (b) –1.15 V. Depth XPS spectra profile of electrodeposited CoNi films from plating bath 2 on Si/Ti/Au electrodes at (c) –1.01 V and (d) –1.15 V.

than that obtained at the more negative potential, suggesting that the presence of oxides increases as the applied potential becomes more negative.

X-ray diffraction was implemented to further confirm the XPS results by investigating the crystal structure of the CoNi films. In Fig. 9 are reported the X-ray diffraction patterns of the CoNi films deposited on Si/Ti/Au electrodes from plating bath 3 – Co14Ni3 (green curve) and bath 4 – Co3Ni14 (purple curve). The most intense diffraction peaks are attributed to cubic Au (38.4° and 82.2°) and cubic Ti (69.2°) of the Si/Ti/Au substrate. Additional relevant peaks are visible in Fig. 9 (right) and were assigned to hexagonal Co (41.7°, 44.8°, 47.5°, 61.7°, 84.6°, and 76.2°) for the CoNi film deposited from plating bath 3, while only Ni cubic phase (44.6°, 51.7°, and 76.3°) was detected in the CoNi film deposited from plating bath 4. The crystal structure of CoNi films therefore seems to be highly dependent on the amount of the Co and Ni metallic species in the alloy. When the Co atomic percentage dominated (i.e., 85 at.% Co), the CoNi films had a slightly distorted Co hexagonal structure, as expected for a Co-rich CoNi solid solution. By contrast, a slightly distorted Ni cubic crystal corresponding to a Ni-rich CoNi solid solution was observed when the Co content was lower (i.e., 13 at.% Co), as shown in Table 2 regarding plating bath 4 (i.e. −0.95 V). Other peaks visible in the magnified X-ray diffractogram belong to the Si/Ti/Au substrate. Therefore, the structural analysis not only confirms the formation of the CoNi alloy in DES medium but it additionally enables to distinguish between different crystal structures of Co and Ni in the alloy depending on the synthesis parameters.

3.4. *Tetracycline degradation*

Once characterized the deposition process reveals that the CoNi alloy

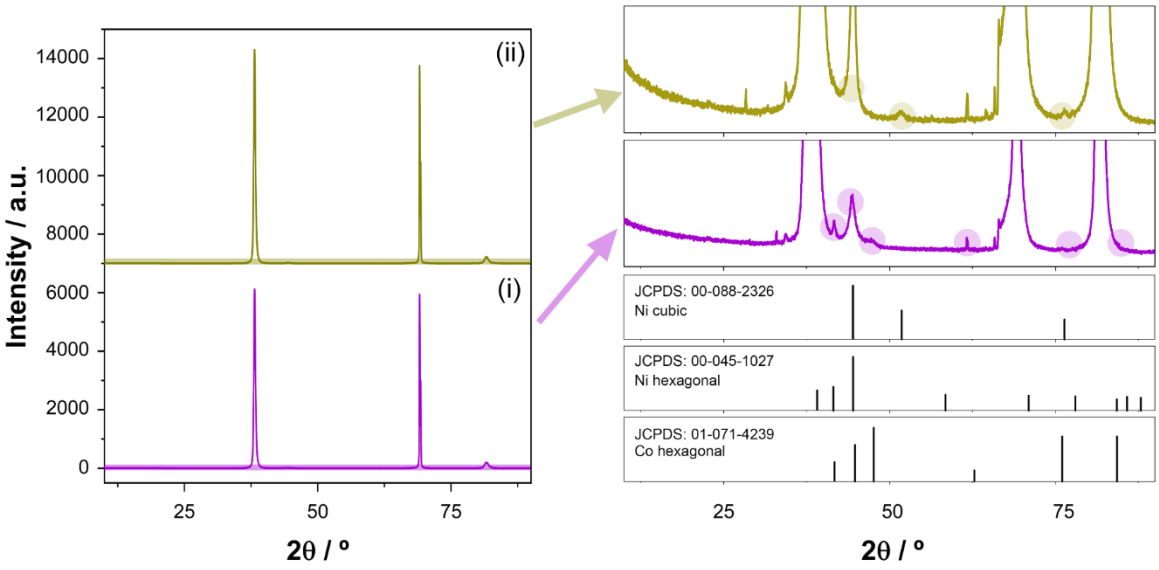

Fig. 9. XRD patterns of electrodeposited CoNi films on Si/Ti/Au electrodes from plating bath 3 at –1.05 V (curve i) and plating bath 4 at –0.95 V (curve ii).

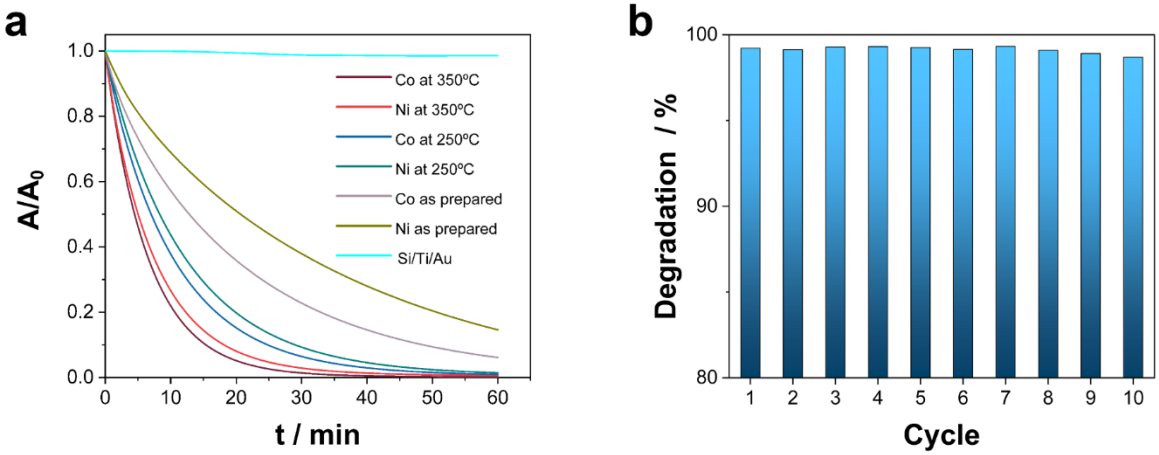

Fig. 10. (a) Degradation of TC using Co-rich and Ni-rich after 60 min at 20 °C. Experimental conditions: 20 ppm of TC, 0.3 mM of PMS, and initial pH = 7.0. (b) Reusability of the Co-rich CoNi (350 °C) deposits in 10 consecutive cycles of 60 min.

could be compositionally tailored *via* applying different electrodeposition conditions; further, these deposits show relative high roughness related mainly to the needled morphology observed, more or less pronounced. In this work, a concept proof is proposed in order to evaluate the suitability of the CoNi deposits obtained, in a new developing application (thus far not tested) and recently proposed for transition metal compounds. The proposal consists in the use of CoNi as an activation platform for promoting the formation of free radicals; in addition, a reactive species, in advanced oxidation processes (AOPs), could be strategic actors for the final mineralization, to CO_2 and H_2O, of organic contaminants. The CoNi system was proposed due to observations that these kinds of platforms containing more than one transition metal have advantages compared with single metal oxides, e.g., improved stability and activity [46–49].

To check the effectivity of CoNi alloy, two different compositions were selected for the formation of sulphate radicals. In order to discriminate the possible prevalent influence of one of the two components, the effect of deposits with around 15% of minority metal was investigated. Potassium peroxomonosulfate (PMS) was the source, *via* scission of the peroxo bond, of sulphate radicals, one, joint with hydroxyl, due to its better performance on organic degradation as a result of its strong oxidant power [46,50–53]. The pollutant selected to be removed in the solution was antibiotic tetracycline [54].

For each CoNi alloy composition, three kinds of deposits were tested, deposits "*as prepared*" and two more subjected to heat treatment. The thermal treatments are used in order to promote the superficial oxides formation, heating at 225 °C and 350 °C, during 2 h in the oven, in all cases preceded by a heating ramp and followed by a controlled cooling ramp.

The degradation of the TC was studied by measuring the absorbance as a function of time with a spectrophotometer (Fig. 10) and the degree of mineralization was verified by measuring the TOC. Experiments of 60 min were considered, in which the TC model solution was 20 ppm at pH = 6, i.e., a pH value selected according to conditions close to those of real contaminated water. The concentration of PMS used in this evaluation was set at 0.3 mM. Absorbance was measured at λ =363 nm, which corresponds to the maximum observed in the tetracycline aqueous solution.

Fig. 10a shows the progressive diminution of the absorbance along the experiment for the six different substrates used, evidencing that, to a greater or lesser extent, all the substrates are capable of promoting the formation of oxidizing species able to degrade the antibiotic, activation, which was demonstrated in blank experiments and does not occur in absence of the activator. The degradation and mineralization of TC using

Table 3
Catalytic performance of CoNi electrodeposits.

Sample	Degradation time	Thermal treatment	Degradation (10 min) / %	Mineralization / %
TC solution	0	–	–	0.0
Si/Ti/Au	60	–	–	0.0
Co-rich	60	As prepared	42.8	72.3
Ni-rich	60	As prepared	31.1	43.6
Co-rich	60	225 °C	62.2	93.0
Ni-rich	60	225 °C	56.3	79.7
Co-rich	60	350 °C	73.4	96.7
Ni-rich	60	350 °C	78.1	91.2

nude Si/Ti/Au substrates as a PMS activator were negligible because the absorbance of TC remained virtually constant over the course of 60 min. Compared with the removal performance of the CoNi deposits, our results indicate that catalysts were more efficient when the deposits were subjected to higher temperatures—that is, their activation improved at higher temperatures in the thermal treatment. The degradation performance triples its value using the heated deposit at 350 °C with respect to the "as-prepared" deposit. It can also be shown that comparing between deposits under the same thermal treatment, Co-rich substrates are slightly more effective than Ni-rich ones. For a semi-quantitative evaluation, it is possible to compare the degradation values recorded at low reaction times (e.g., after 10 min of degradation), conditions in which the TC in solution is not zero. Degradation followed the same trend; the higher the temperature of the heat treatment applied to the deposits, the better the catalytic activity. At the same time, the catalytic activity of Co-rich deposits was also always higher. Catalytic efficiency was also evaluated by TOC in order to measure the organic carbon removed during the TC degradation process. Table 3 summarizes the results. Beyond that, Fig. 10b shows the reusability experiments of the Co-rich CoNi (350 °C) deposits within 10 successive runs of PMS catalysis. The degradation remained virtually constant (i.e., approx. 100%) after 10 consecutive runs, which indicates the favorable reusability potential of the as-synthesized catalysts within successive runs of operation.

The results in Table 3 show that after 60 min of TC degradation, all substrates are effective at mineralizing. Comparing the results for the same Co/Ni ratio, it is clear that deposits treated at higher temperatures mineralize more effectively. However, although from the degradation behavior it seemed that the thermal treatment was the driving factor, this is not entirely true for mineralization, since it seems clear that not only the thermal treatment is important, but also the composition. These preliminary results encourage a more complete study of these materials as activators, taking advantage of the fact that the preparation method is versatile, which allows designing the composition of the material on demand and, where appropriate, enhancing the roughness of the deposit.

4. Conclusions

In sum, the study involved systematically analyzing the process of electrodeposition of nanostructured CoNi alloyed films in a biocompatible DES. Depending on the parameters of synthesis, especially the concentration of Ni and Co salts in the plating bath, homogeneous, continuous, and needle-shaped deposits with randomly distributed sharper edges were obtained. The grains formed a network structure with an interwoven morphology, which became smaller as the Ni content in the deposit increased. The applied potential also influenced the chemical nature of the deposits, for when the solvent co-reduced at more negative potentials, oxygen species became incorporated into the deposits. Beyond that, the CoNi alloyed films presented two CoNi alloyed crystal structures; whereas both Co and Ni had a hexagonal structure amid high (85%) Co atomic content, a low amount of Co content (13 at. %) promoted the formation of Ni cubic crystalline structures and amorphous Co nanocrystalline structures. The parameters of electrosynthesis, including bath composition, allowed the strict control of deposit morphology, elemental composition, and crystal structure and size. CoNi's nature as well as the surface morphology of the deposits provided abundant exposed edges and sharp corners that facilitated the rapid transport and migration of PMS and consequently guaranteed the effective formation of highly reactive sulfate radicals. CoNi alloyed films, especially after undergoing thermal treatment in the presence of oxygen and, in turn, promoting the formation of oxo and hydroxo Co and Ni species, thus emerge as a platform for activating PMS and consequently mineralizing organic contaminants such as tetracycline. Altogether, electrochemical media, electrosynthesis, and nanostructured CoNi alloyed materials may be especially relevant for synthesizing more effective catalysts for decontaminating water *via* PMS catalysis.

CRediT authorship contribution statement

Elvira Gómez: Conceptualization, Methodology, Conceptualization, Investigation, Software, Data curation, Validation, Funding acquisition, Project administration, Resources, Writing – original draft, Writing – review & editing. **Arnau Fons:** Conceptualization, Methodology, Formal analysis, Data curation, Writing – original draft. **Roberto Cestaro:** Conceptualization, Methodology, Formal analysis, Data curation, Writing – original draft. **Albert Serrà:** Conceptualization, Methodology, Conceptualization, Investigation, Software, Data curation, Validation, Funding acquisition, Project administration, Resources, Writing – original draft, Writing – review & editing.

Declaration of Competing Interest

The authors declare that they have no known competing financial interests or personal relationships that could have appeared to influence the work reported in this paper.

Data availability

No data was used for the research described in the article.

Acknowledgments

Grant PID2020-115663GB-C32 funded by MCIN/ AEI /10.13039/501100011033. Authors thank the CCiT-UB for the use of their equipment. The authors also acknowledge the contribution of Amber Breakspear Erasmus student.

Supplementary materials

Supplementary material associated with this article can be found, in the online version, at doi:10.1016/j.electacta.2022.141428.

References

[1] W. Sides, N. Kassouf, Q. Huang, Electrodeposition of ferromagnetic FeCo and FeCoMn alloy from choline chloride based deep eutectic solvent, J. Electrochem. Soc. 166 (2019) D77–D85, https://doi.org/10.1149/2.0181904jes.

[2] F.G.S. Oliveira, F. Bohn, A.N. Correia, I.F. Vasconcelos, P. de Lima-Neto, Fe–Co coatings electrodeposited from eutectic mixture of choline chloride-urea: physical characterizations and evaluation as electrocatalysts for the hydrogen evolution reaction, J. Alloys Compd. 851 (2021), https://doi.org/10.1016/j.jallcom.2020.156330.

[3] A. Karpuz, H. Kockar, M. Alper, Effect of film thickness on properties of electrodeposited Ni-Co films, Appl. Surf. Sci. 258 (2012) 5046–5051, https://doi.org/10.1016/j.apsusc.2012.01.083.

[4] J. García-Torres, E. Gómez, E. Vallés, Modulation of magnetic and structural properties of cobalt thin films by means of electrodeposition, J. Appl. Electrochem. 39 (2009) 233–240, https://doi.org/10.1007/s10800-008-9661-9.

[5] L. Zhang, D.P. Wilkinson, Y. Liu, J. Zhang, Progress in nanostructured (Fe or Co)/N/C non-noble metal electrocatalysts for fuel cell oxygen reduction reaction, Electrochim. Acta 262 (2018) 326–336, https://doi.org/10.1016/j.electacta.2018.01.046.

[6] S. Wang, X. Zou, Y. Lu, S. Rao, X. Xie, Z. Pang, X. Lu, Q. Xu, Z. Zhou, Electrodeposition of nano-nickel in deep eutectic solvents for hydrogen evolution reaction in alkaline solution, Int. J. Hydrogen Energy 43 (2018) 15673–15686, https://doi.org/10.1016/j.ijhydene.2018.06.188.

[7] A. Serrà, E. Gómez, M. Montiel, E. Vallés, Effective new method for synthesizing Pt and $CoPt_3$ mesoporous nanorods. New catalysts for ethanol electro-oxidation in alkaline medium, RSC Adv. 6 (2016) 47931–47939, https://doi.org/10.1039/C6RA06407H.

[8] I. El-Hallag, S. Elsharkawy, S. Hammad, Electrodeposition of Ni nanoparticles from deep eutectic solvent and aqueous solution as electrocatalyst for methanol oxidation in acidic media, Int. J. Hydrogen Energy 46 (2021) 15442–15453, https://doi.org/10.1016/j.ijhydene.2021.02.049.

[9] G.F. Cai, J.P. Tu, C.D. Gu, J.H. Zhang, J. Chen, D. Zhou, S.J. Shi, X.L. Wang, One-step fabrication of nanostructured NiO films from deep eutectic solvent with enhanced electrochromic performance, J. Mater. Chem. A 1 (2013) 4286–4292, https://doi.org/10.1039/c3ta01055d.

[10] H. Li, F. Musharavati, E. Zalenezhad, X. Chen, K.N. Hui, K.S. Hui, Electrodeposited Ni–Co layered double hydroxides on titanium carbide as a binder-free electrode for supercapacitors, Electrochim. Acta 261 (2018) 178–187, https://doi.org/10.1016/j.electacta.2017.12.139.

[11] E. Gómez, S. Pané, E. Vallés, Magnetic composites CoNi-barium ferrite prepared by electrodeposition, Electrochem. Commun. 7 (2005) 1225–1231, https://doi.org/10.1016/j.elecom.2005.08.016.

[12] J. García-Torres, A. Serrà, P. Tierno, X. Alcobé, E. Vallés, Magnetic propulsion of recyclable catalytic nanocleaners for pollutant degradation, ACS Appl. Mater. Interfaces 9 (2017), https://doi.org/10.1021/acsami.7b07480.

[13] A. Serrà, E. Gómez, G. Calderó, J. Esquena, C. Solans, E. Vallés, Conductive microemulsions for template CoNi electrodeposition, Phys. Chem. Chem. Phys. 15 (2013), https://doi.org/10.1039/c3cp52021h.

[14] A. Karpuz, H. Kockar, M. Alper, O. Karaagac, M. Haciismailoglu, Electrodeposited Ni-Co films from electrolytes with different Co contents, Appl. Surf. Sci. 258 (2012) 4005–4010, https://doi.org/10.1016/j.apsusc.2011.12.088.

[15] J. Vazquez-Arenas, T. Treeratanaphitak, M. Pritzker, Formation of Co-Ni alloy coatings under direct current, pulse current and pulse-reverse plating conditions, Electrochim. Acta 62 (2012) 63–72, https://doi.org/10.1016/j.electacta.2011.11.085.

[16] W. Li, J. Hao, W. Liu, S. Mu, Electrodeposition of nano Ni–Co alloy with (220) preferred orientation from choline chloride-urea: electrochemical behavior and nucleation mechanism, J. Alloys Compd. 853 (2021), https://doi.org/10.1016/j.jallcom.2020.157158.

[17] J. Vazquez-Arenas, L. Altamirano-Garcia, T. Treeratanaphitak, M. Pritzker, R. Luna-Sánchez, R. Cabrera-Sierra, Co-Ni alloy electrodeposition under different conditions of pH, current and composition, Electrochim. Acta 65 (2012) 234–243, https://doi.org/10.1016/j.electacta.2012.01.050.

[18] L. Tian, J. Xu, C. Qiang, The electrodeposition behaviors and magnetic properties of Ni-Co films, Appl. Surf. Sci. 257 (2011) 4689–4694, https://doi.org/10.1016/j.apsusc.2010.12.123.

[19] E. Gómez, J. Ramirez, E. Vallés, Electrodeposition of Co-Ni alloys, J. Appl. Electrochem. 28 (1998) 71–79, https://doi.org/10.1023/A:1003201919054.

[20] J. Vijayakumar, S. Mohan, S. Anand Kumar, S.R. Suseendiran, S. Pavithra, Electrodeposition of Ni-Co-Sn alloy from choline chloride-based deep eutectic solvent and characterization as cathode for hydrogen evolution in alkaline solution, Int. J. Hydrogen Energy 38 (2013) 10208–10214, https://doi.org/10.1016/j.ijhydene.2013.06.068.

[21] X. He, Z. Sun, Q. Zou, J. Yang, L. Wu, Codeposition of nanocrystalline Co-Ni catalyst based on 1-ethyl-3-methylimidazolium bisulfate and ethylene glycol system for hydrogen evolution reaction, J. Electrochem. Soc. 166 (2019) D908–D915, https://doi.org/10.1149/2.0171916jes.

[22] A.P. Abbott, A. Ballantyne, R.C. Harris, J.A. Juma, K.S. Ryder, Bright metal coatings from sustainable electrolytes: the effect of molecular additives on electrodeposition of nickel from a deep eutectic solvent, Phys. Chem. Chem. Phys. 19 (2017) 3219–3231, https://doi.org/10.1039/c6cp08720e.

[23] A.P. Abbott, A. Ballantyne, R.C. Harris, J.A. Juma, K.S. Ryder, A comparative study of nickel electrodeposition using deep eutectic solvents and aqueous solutions, Electrochim. Acta 176 (2015) 718–726, https://doi.org/10.1016/j.electacta.2015.07.051.

[24] M. Srivastava, G. Yoganandan, V.K. William Grips, Electrodeposition of Ni and Co coatings from ionic liquid, Surf. Eng. 28 (2012) 424–429, https://doi.org/10.1179/1743294412Y.0000000008.

[25] A.P. Abbott, G. Capper, D.L. Davies, R.K. Rasheed, V. Tambyrajah, Novel solvent properties of choline chloride/urea mixtures, Chem. Commun. (2003) 70–71, https://doi.org/10.1039/b210714g.

[26] L.I.N. Tomé, V. Baião, W. da Silva, C.M.A. Brett, Deep eutectic solvents for the production and application of new materials, Appl. Mater. Today 10 (2018) 30–50, https://doi.org/10.1016/j.apmt.2017.11.005.

[27] M. Lukaczynska, E.A. Mernissi Cherigui, A. Ceglia, K. Van Den Bergh, J. De Strycker, H. Terryn, J. Ustarroz, Influence of water content and applied potential on the electrodeposition of Ni coatings from deep eutectic solvents, Electrochim. Acta 319 (2019) 690–704, https://doi.org/10.1016/j.electacta.2019.06.161.

[28] E.A.M. Cherigui, K. Sentosun, M.H. Mamme, M. Lukaczynska, H. Terryn, S. Bals, J. Ustarroz, On the control and effect of water content during the electrodeposition of Ni nanostructures from deep eutectic solvents, J. Phys. Chem. C 122 (2018) 23129–23142, https://doi.org/10.1021/acs.jpcc.8b05344.

[29] P. Sebastian, M.I. Giannotti, E. Gómez, J.M. Feliu, Surface sensitive nickel electrodeposition in deep eutectic solvent, ACS Appl. Energy Mater. 1 (2018) 1016–1028, https://doi.org/10.1021/acsaem.7b00177.

[30] Y.H. You, C.D. Gu, X.L. Wang, J.P. Tu, Electrodeposition of Ni-Co alloys from a deep eutectic solvent, Surf. Coat. Technol. 206 (2012) 3632–3638, https://doi.org/10.1016/j.surfcoat.2012.03.001.

[31] W. Li, J. Hao, S. Mu, W. Liu, Electrochemical behavior and electrodeposition of Ni-Co alloy from choline chloride-ethylene glycol deep eutectic solvent, Appl. Surf. Sci. 507 (2020), https://doi.org/10.1016/j.apsusc.2019.144889.

[32] M. Landa-Castro, J. Aldana-González, M.G. Montes de Oca-Yemha, M. Romero-Romo, E.M. Arce-Estrada, M. Palomar-Pardavé, Ni–Co alloy electrodeposition from the cathode powder of Ni-MH spent batteries leached with a deep eutectic solvent (reline), J. Alloys Compd. 830 (2020) 1–9, https://doi.org/10.1016/j.jallcom.2020.154650.

[33] T. Shi, X. Zou, S. Wang, Z. Pang, W. Tang, G. Li, Q. Xu, X. Lu, Electrodeposition of Sn-Co-Ni and Sn-Co-Zn alloy coatings on copper substrate in a deep eutectic solvent and their characterization, Int. J. Electrochem. Sci. 15 (2020) 7493–7507, https://doi.org/10.20964/2020.08.27.

[34] M. Landa-Castro, P. Sebastián, M.I. Giannotti, A. Serrà, E. Gómez, Electrodeposition of nanostructured cobalt films from a deep eutectic solvent: influence of the substrate and deposition potential range, Electrochim. Acta 359 (2020), https://doi.org/10.1016/j.electacta.2020.136928.

[35] A. Serrà, P. Sebastián-Pascual, M. Landa-Castro, E. Gómez, Electrochemical assessment of high active area of cobalt deposited in deep eutectic solvent, J. Electroanal. Chem. 896 (2021), https://doi.org/10.1016/j.jelechem.2021.115177.

[36] A. Florea, L. Anicai, S. Costovici, F. Golgovici, T. Visan, Ni and Ni alloy coatings electrodeposited from choline chloride-based ionic liquids - electrochemical synthesis and characterization, Surf. Interface Anal. 42 (2010) 1271–1275, https://doi.org/10.1002/sia.3317.

[37] R.D.C. Soltani, M. Mashayekhi, M. Naderi, G. Boczkaj, S. Jorfi, M. Safari, Sonocatalytic degradation of tetracycline antibiotic using zinc oxide nanostructures loaded on nano-cellulose from waste straw as nanosonocatalyst, Ultrason. Sonochem. 55 (2019) 117–124, https://doi.org/10.1016/j.ultsonch.2019.03.009.

[38] F. Chen, G.X. Huang, F.B. Yao, Q. Yang, Y.M. Zheng, Q.B. Zhao, H.Q. Yu, Catalytic degradation of ciprofloxacin by a visible-light-assisted peroxymonosulfate activation system: performance and mechanism, Water Res. 173 (2020), 115559, https://doi.org/10.1016/j.watres.2020.115559.

[39] J. Deng, Y. Ge, C. Tan, H. Wang, Q. Li, S. Zhou, K. Zhang, Degradation of ciprofloxacin using A-MnO_2 activated peroxymonosulfate process: effect of water constituents, degradation intermediates and toxicity evaluation, Chem. Eng. J. 330 (2017) 1390–1400, https://doi.org/10.1016/j.cej.2017.07.137.

[40] M.G. Antoniou, I. Boraei, M. Solakidou, Y. Deligiannakis, M. Abhishek, L. A. Lawton, C. Edwards, Enhancing photocatalytic degradation of the cyanotoxin microcystin-LR with the addition of sulfate-radical generating oxidants, J. Hazard. Mater. 360 (2018) 461–470, https://doi.org/10.1016/j.jhazmat.2018.07.111.

[41] O.S. Hammond, D.T. Bowron, K.J. Edler, Liquid structure of the choline chloride-urea deep eutectic solvent (reline) from neutron diffraction and atomistic modelling, Green Chem. 18 (2016) 2736–2744, https://doi.org/10.1039/c5gc02914g.

[42] Q. Li, H. Qian, X. Fu, H. Sun, J. Sun, Characterization and electrochemical analysis of silver electrodeposition in ChCl–urea deep eutectic solvents, Bull. Mater. Sci. 44 (2021), https://doi.org/10.1007/s12034-020-02276-3.

[43] F.R. Bento, L.H. Mascaro, Electrocrystallisation of Fe-Ni alloys from chloride electrolytes, Surf. Coat. Technol. 201 (2006) 1752–1756, https://doi.org/10.1016/j.surfcoat.2006.02.055.

[44] E.A. Mernissi Cherigui, K. Sentosun, P. Bouckenooge, H. Vanrompay, S. Bals, H. Terryn, J. Ustarroz, Comprehensive study of the electrodeposition of nickel nanostructures from deep eutectic solvents: self-limiting growth by electrolysis of residual water, J. Phys. Chem. C 121 (2017) 9337–9347, https://doi.org/10.1021/acs.jpcc.7b01104.

[45] D. Coviello, M. Contursi, R. Toniolo, I.G. Casella, Electrochemical and spectroscopic investigation of a binary Ni-Co oxide active material deposited on graphene/polyvinyl alcohol composite substrate, J. Electroanal. Chem. 791 (2017) 117–123, https://doi.org/10.1016/j.jelechem.2017.02.048.

[46] J. Li, G. Gou, H. Zhao, C. Liu, N. Li, L. Li, B. Tan, B. Lai, Efficient peroxymonosulfate activation by $CoFe_2O_4$-CeO_2 composite: performance and catalytic mechanism, Chem. Eng. J. 435 (2022), 134840, https://doi.org/10.1016/j.cej.2022.134840.

[47] H.T. Nguyen, J. Lee, E. Kwon, G. Lisak, B.X. Thanh, F. Ghanbari, K.Y.A. Lin, Bamboo-like N-doped carbon nanotube–confined cobalt as an efficient and robust

catalyst for activating monopersulfate to degrade bisphenol A, Chemosphere 279 (2021), 130569, https://doi.org/10.1016/j.chemosphere.2021.130569.
[48] Z. Huang, P. Wu, C. Liu, M. Chen, S. Yang, Z. Dang, N. Zhu, Multiple catalytic reaction sites induced non-radical/radical pathway with graphene layers encapsulated Fe-N-C toward highly efficient peroxymonosulfate (PMS) activation, Chem. Eng. J. 413 (2021), 127507, https://doi.org/10.1016/j.cej.2020.127507.
[49] H. Xu, D. Wang, J. Ma, T. Zhang, X. Lu, Z. Chen, A superior active and stable spinel sulfide for catalytic peroxymonosulfate oxidation of bisphenol S, Appl. Catal. B Environ. 238 (2018) 557–567, https://doi.org/10.1016/j.apcatb.2018.07.058.
[50] Y. Song, D. Sun, X. Jiang, H. Ma, C. Ma, J. Hao, X. Zhang, Enhanced activation of peroxymonosulfate by bimetallic spinel sulfides $CoNi_2S_4$ for organic dye degradation, J. Environ. Chem. Eng. 9 (2021), 106889, https://doi.org/10.1016/j.jece.2021.106889.
[51] X. Zhou, Q. Zhao, J. Wang, Z. Chen, Z. Chen, Nonradical oxidation processes in PMS-based heterogeneous catalytic system: generation, identification, oxidation characteristics, challenges response and application prospects, Chem. Eng. J. 410 (2021), 128312, https://doi.org/10.1016/j.cej.2020.128312.
[52] L. Chen, H. Ji, J. Qi, T. Huang, C.C. Wang, W. Liu, Degradation of acetaminophen by activated peroxymonosulfate using $Co(OH)_2$ hollow microsphere supported titanate nanotubes: Insights into sulfate radical production pathway through $CoOH^+$ activation, Chem. Eng. J. 406 (2021), 126877, https://doi.org/10.1016/j.cej.2020.126877.
[53] Z. Sun, X. Liu, X. Dong, X. Zhang, Y. Tan, F. Yuan, S. Zheng, C. Li, Synergistic activation of peroxymonosulfate *via in situ* growth $FeCo_2O_4$ nanoparticles on natural rectorite: role of transition metal ions and hydroxyl groups, Chemosphere 263 (2021), 127965, https://doi.org/10.1016/j.chemosphere.2020.127965.
[54] A. Bembibre, M. Benamara, M. Hjiri, E. Gómez, H.R. Alamri, R. Dhahri, A. Serrà, Visible-light driven sonophotocatalytic removal of tetracycline using Ca-doped ZnO nanoparticles, Chem. Eng. J. 427 (2022), https://doi.org/10.1016/j.cej.2021.132006.